Solar Sail Deployment Dynamics

Behrad Vatankhahghadim[1] and Christopher J. Damaren[1]

[1] *Institute for Aerospace Studies, University of Toronto, {behrad.vatankhahghadim@mail , damaren@utias}.utoronto.ca*

The deployment dynamics and vibration characteristics of a flexible multibody system, namely a solar sail consisting of four thin membrane quadrants (with negligible bending stiffness) and four flexible booms (approximated as Euler-Bernoulli beams), shown in Fig. 1, are studied. The ultimate objective is to further the mathematical understanding behind the transient dynamics of solar sails, hence facilitating their design and successful deployment.

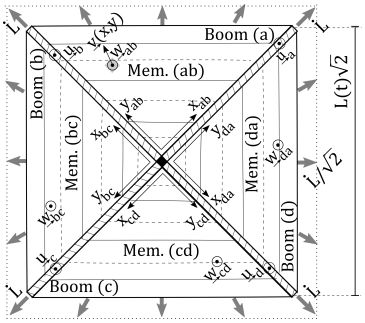

Fig. 1: Deploying Solar Sail Model

In [1], a separate work upon which the present paper builds, the out-of-plane deflections of two booms, $u_{\mathrm{a}}(x_{\mathrm{ab}},t)$ or $u_{\mathrm{b}}(y_{\mathrm{ab}},t)$, and that of the membrane quadrant in-between, $w_{\mathrm{ab}}(x_{\mathrm{ab}},y_{\mathrm{ab}},t)$ (superimposed over the booms' deflections as in [2]) are expanded, using n_{B} and n_{M} modes, respectively, as:

$$u_{\mathrm{a}}(x_{\mathrm{ab}},t)=\mathbf{p}_{\mathrm{a}}^{\mathsf{T}}(t)\boldsymbol{\Psi}_{\mathrm{a}}(x_{\mathrm{ab}},t)\ ,\ u_{\mathrm{b}}(y_{\mathrm{ab}},t)=\mathbf{p}_{\mathrm{b}}^{\mathsf{T}}(t)\boldsymbol{\Psi}_{\mathrm{b}}(y_{\mathrm{ab}},t)\ ,\ w_{\mathrm{ab}}(x_{\mathrm{ab}},y_{\mathrm{ab}},t)=u_{\mathrm{a}}+u_{\mathrm{b}}+\mathbf{q}_{\mathrm{ab}}^{\mathsf{T}}(t)\boldsymbol{\Phi}_{\mathrm{ab}}(x_{\mathrm{ab}},y_{\mathrm{ab}},t) \quad (1)$$

where $\mathbf{p}_{\mathrm{a}}\in\mathbb{R}^{n_{\mathrm{B}}}$, $\mathbf{p}_{\mathrm{b}}\in\mathbb{R}^{n_{\mathrm{B}}}$, and $\mathbf{q}_{\mathrm{ab}}\in\mathbb{R}^{n_{\mathrm{M}}}$ are the time-varying generalized coordinates of Boom (a), Boom (b) and Membrane (ab), respectively. The components of $\boldsymbol{\Psi}$ and $\boldsymbol{\Phi}$ are the eigenfunctions of a cantilevered beam and a clamped membrane, which are time-varying for they depend on $x_{\mathrm{ab}}/L(t)$ and/or $y_{\mathrm{ab}}/L(t)$. A similar approach (but for one-dimensional beam motion) was used in [3], among others. The following discretized equations of motion for a single sail quadrant consisting of Membrane (ab) attached to Booms (a) and (b) were obtained in [1]:

$$\left[\tilde{\mathbf{M}}_{\mathrm{M}}+\tilde{\mathbf{M}}_{\mathrm{B}}\right]\ddot{\tilde{\mathbf{q}}}+\left[\left(\dot{\tilde{\mathbf{M}}}_{\mathrm{M}}+\dot{\tilde{\mathbf{M}}}_{\mathrm{B}}\right)+\left(\tilde{\mathbf{G}}_{\mathrm{M}}-\tilde{\mathbf{G}}_{\mathrm{M}}^{\mathsf{T}}\right)+\left(\tilde{\mathbf{G}}_{\mathrm{B}}-\tilde{\mathbf{G}}_{\mathrm{B}}^{\mathsf{T}}\right)\right]\dot{\tilde{\mathbf{q}}}+\left[\left(\dot{\tilde{\mathbf{G}}}_{\mathrm{M}}+\dot{\tilde{\mathbf{G}}}_{\mathrm{B}}\right)+\left(\Delta\tilde{\mathbf{K}}_{\mathrm{M}}+\Delta\tilde{\mathbf{K}}_{\mathrm{B}}\right)\right]\tilde{\mathbf{q}}=\mathbf{0} \quad (2)$$

where $\tilde{\mathbf{q}}\triangleq[\,\mathbf{p}_{\mathrm{a}}^{\mathsf{T}}\ \ \mathbf{p}_{\mathrm{b}}^{\mathsf{T}}\ \ \mathbf{q}_{\mathrm{ab}}^{\mathsf{T}}\,]^{\mathsf{T}}$ contains all of the $\mathrm{Q_{ab}}$ quadrant's generalized coordinates. The quadrant-level matrices denoted by a tilde are $\tilde{n}\times\tilde{n}$ with $\tilde{n}=2n_{\mathrm{B}}+n_{\mathrm{M}}$, and are constructed via spatial integration of some functions of $\boldsymbol{\Psi}$ and $\boldsymbol{\Phi}$, as detailed in [1]. Recognizing a need for completeness in modelling and simulation, the present work first provides more details on extending the above formulation to a complete four-quadrant sail. To this end, the quadrant-level matrices are "lifted" into system-level forms that correspond to the system-level collection of *all* generalized coordinates, $\bar{\mathbb{q}}\triangleq[\,\mathbf{p}_{\mathrm{a}}^{\mathsf{T}}\ \ \mathbf{p}_{\mathrm{b}}^{\mathsf{T}}\ \ \mathbf{p}_{\mathrm{c}}^{\mathsf{T}}\ \ \mathbf{p}_{\mathrm{d}}^{\mathsf{T}}\ \ \mathbf{q}_{\mathrm{ab}}^{\mathsf{T}}\ \ \mathbf{q}_{\mathrm{bc}}^{\mathsf{T}}\ \ \mathbf{q}_{\mathrm{cd}}^{\mathsf{T}}\ \ \mathbf{q}_{\mathrm{da}}^{\mathsf{T}}\,]^{\mathsf{T}}$. First, each of the quadrant-level matrices are partitioned into nine submatrices (for example $\tilde{\mathbf{M}}_{\mathrm{M,ab},ij}$ with $i,j\in\{1,2,3\}$) that correspond to $\mathbf{p}_{\mathrm{a}}$, $\mathbf{p}_{\mathrm{b}}$, and $\mathbf{q}_{\mathrm{ab}}$.The system-level mass matrix corresponding to the $\mathrm{Q_{ab}}$ quadrant's membrane, denoted by $\bar{\mathbb{M}}_{\mathrm{M,ab}}$ and of dimensions $\bar{n}\times\bar{n}$ with $\bar{n}=4n_{\mathrm{B}}+4n_{\mathrm{M}}$, can be partitioned into 64 blocks, namely $\bar{\mathbb{M}}_{\mathrm{M,ab},pq}$ with $p,q\in\{1,\cdots,8\}$. Of these 64 blocks, nine are replaced by $\tilde{\mathbf{M}}_{\mathrm{M,ab},ij}$, and the rest are all zero matrices of appropriate dimensions. Summarized in Tab. 1 is the mapping between the indices of the quadrant-level matrices and those of the system-level matrices. For example, the $\tilde{\mathbf{M}}_{\mathrm{M,ab},23}$ block of the quadrant-level $\tilde{\mathbf{M}}_{\mathrm{M,ab}}$ replaces the $\bar{\mathbb{M}}_{\mathrm{M,ab},25}$ block of the system-level $\bar{\mathbb{M}}_{\mathrm{M,ab}}$, and so on. Lastly, after all of the matrices in Eq. (2) for all four quadrants are lifted into their system-level form using the above procedure and the mapping in Tab. 1, the overall system matrices are computed by simple addition. For example, the membranes' total mass matrix is given by $\bar{\mathbb{M}}_{\mathrm{M}}=\bar{\mathbb{M}}_{\mathrm{M,ab}}+\bar{\mathbb{M}}_{\mathrm{M,bc}}+\bar{\mathbb{M}}_{\mathrm{M,cd}}+\bar{\mathbb{M}}_{\mathrm{M,da}}$. The resulting system matrices replace their quadrant-level counterparts in Eq. (2) to describe the complete system's dynamics.

Quadrant	$\mathrm{Q_{ab}}$			$\mathrm{Q_{bc}}$			$\mathrm{Q_{cd}}$			$\mathrm{Q_{da}}$		
Quadrant-Level (i,j)	1	2	3	1	2	3	1	2	3	1	2	3
System-Level (p,q)	1	2	5	2	3	6	3	4	7	4	1	8

Tab. 1: Mapping between Block Indices of the Partitioned Quadrant-Level and System-Level Matrices

Modal Frequency	ω_1	ω_2	ω_3	ω_4	ω_5	ω_6
Using FEM [4] (rad/s)	0.05180	0.20848	0.20848	0.30520	0.36781	0.36781
Present Method (rad/s)	0.05328	0.20954	0.20954	0.31002	0.37091	0.37091

Tab. 2: Comparison of the Modal Frequencies (for Fully-Deployed Sail) Obtained Using the Present Approach vs. FEM in [4]

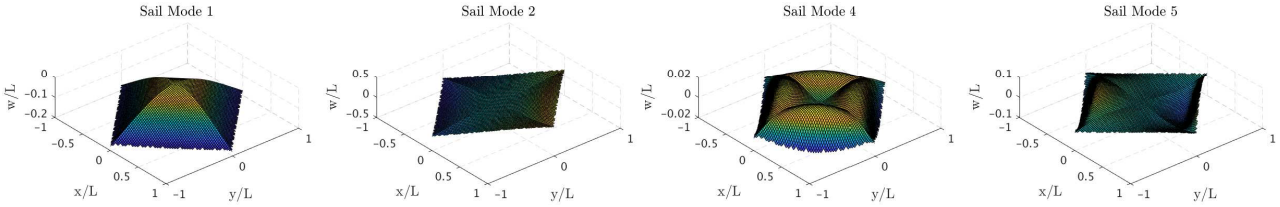

Fig. 2: First Four Distinct Modes of Solar Sail with Boom Length $L = 50\sqrt{2}$ m (for Comparison with Figure 6 in [4])

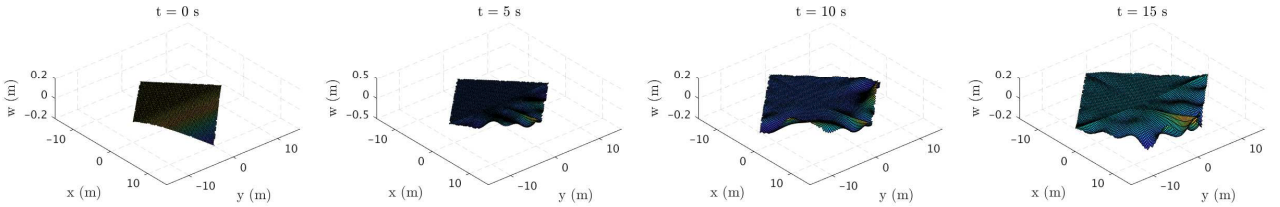

Fig. 3: Snapshots of Simulated Sail Deployment Process (from $L_0 = 10$ m to $L_f = 15$ m in 15 s)

Before studying deployment, validation of the basics of the modelling and simulation using past literature is in order. To this end, the mode shapes and frequencies of the entire sail, after full deployment into a 100 m $\times$ 100 m square shape, are compared against those obtained in [4] using the different formulation of finite element method (FEM), assuming the same geometric and physical parameters for the sail. The first 6 modal frequencies (obtained upon neglecting axial tension imposed on the booms, consistent with [4]) as listed in Tab. 2 show less than 3% discrepancy compared with those reported in [4], and the associated mode shapes (corresponding to the distinct frequencies) presented in Fig. 2 resemble those in [4]. As expected, the complete sail has additional symmetric/anti-symmetric modes that would not appear in the single sail quadrant considered in [1]. Given that a primary contribution of this paper is deployment studies of a solar sail with time-varying boom lengths, a sample deployment sequence with a realistic extension profile (with initial displacement on one boom) is depicted in Fig. 3.

Also to be presented are numerical studies on the effects of varying the system's geometric and physical properties. To this end, the system-level analogue of Eq. (2) is recast into first-order form (as in [5] for FEM):

$$\bar{\mathbb{M}}_{\text{eq}}\ddot{\bar{\mathbf{q}}}+\bar{\mathbb{G}}_{\text{eq}}\dot{\bar{\mathbf{q}}}+\bar{\mathbb{K}}_{\text{eq}}\bar{\mathbf{q}}=\mathbf{0} \;\Rightarrow\; \begin{bmatrix}\bar{\mathbb{M}}_{\text{eq}} & \mathbf{0}\\ \mathbf{0} & \bar{\mathbb{M}}_{\text{eq}}\end{bmatrix}\dot{\bar{\mathbf{x}}}+\begin{bmatrix}\bar{\mathbb{G}}_{\text{eq}} & \bar{\mathbb{K}}_{\text{eq}}\\ -\bar{\mathbb{M}}_{\text{eq}} & \mathbf{0}\end{bmatrix}\bar{\mathbf{x}}=\mathbf{0} \tag{3}$$

where $\bar{\mathbf{x}} \triangleq [\ \dot{\bar{\mathbf{q}}}^{\mathsf{T}}\ \ \bar{\mathbf{q}}^{\mathsf{T}}\ ]^{\mathsf{T}}$. The eigenvalues of the resulting system are then plotted as functions of the membrane prestress (for various extension rates) to determine the on-set of dynamic instability (if there is any).

References

[1] B. Vatankhahghadim and C. J. Damaren, "Deployment dynamics and stability analysis of a membrane attached to two axially-moving beams," *Journal of Sound and Vibration*, Submitted in January 2018.

[2] G. E. Weeks, "Dynamic analysis of a deployable space structure," *Journal of Spacecraft and Rockets*, vol. 23, no. 1, pp. 102–107, 1986.

[3] B. Tabarrok, C. M. Leech, and Y. I. Kim, "On the dynamics of an axially moving beam," *Journal of the Franklin Institute*, vol. 297, no. 3, pp. 201–220, Mar. 1974.

[4] S. Hassanpour and C. J. Damaren, "Linear structural dynamics and modal cost analysis for a solar sail," in *Guidance, Navigation, and Control Conference, SciTech Forum*, pp. 1–19, January 8 – 12, Kissimmee, Florida, USA 2018.

[5] J. Niemi and A. Pramila, "FEM-analysis of transverse vibrations of an axially moving membrane immersed in ideal fluid," *International Journal for Numerical Methods in Engineering*, vol. 24, pp. 2301–2313, Dec. 1987.